

## ARTICLE OPEN

Signature of multilayer growth of 2D layered  $\text{Bi}_2\text{Se}_3$  through heteroatom-assisted step-edge barrier reductionYongsam Kim<sup>1,4</sup>, Geunsik Lee<sup>2,4</sup>, Nannan Li<sup>2</sup>, Jikeun Seo<sup>3</sup>, Kwang S. Kim<sup>2\*</sup> and Namdong Kim<sup>1\*</sup>

During growth of two-dimensional (2D) materials, abrupt growth of multilayers is practically unavoidable even in the case of well-controlled growth. In epitaxial growth of a quintuple-layered  $\text{Bi}_2\text{Se}_3$  film, we observe that the multilayer growth pattern deduced from in situ x-ray diffraction implies nontrivial interlayer diffusion process. Here we find that an intriguing diffusion process occurs at step edges where a slowly downward-diffusing Se adatom having a high step-edge barrier interacts with a Bi adatom pre-existing at step edges. The Se–Bi interaction lowers the high step-edge barrier of Se adatoms. This drastic reduction of the overall step-edge barrier and hence increased interlayer diffusion modifies the overall growth significantly. Thus, a step-edge barrier reduction mechanism assisted by hetero adatom–adatom interaction could be fairly general in multilayer growth of 2D heteroatomic materials.

npj 2D Materials and Applications (2019)3:51 ; <https://doi.org/10.1038/s41699-019-0134-2>

## INTRODUCTION

Two-dimensional (2D) layered materials generally have weak van der Waals (vdW) interactions between layers.<sup>1–4</sup> These systems possess strong anisotropic properties that are exploited to tailor optoelectronic, spintronic, and thermoelectric devices to meet practical requirements.<sup>5,6</sup> Sizable growth of 2D atomic layers in high quality is required for application and it will be enabled by optimizing the growth kinetic parameters. The overall patterns of simple epitaxial growth have been explained with growth parameters such as interlayer diffusion, terrace diffusion, and 2D nucleation within the framework of the standard kinetic multilayer growth model.<sup>7–9</sup> During complex layered-material growth, density of mobile atoms is enhanced on the dimensionally reduced surface, especially near steps that occur at the lateral-growth-front of islands on surface. In this situation, a simple hopping model of free adatoms may fail to describe the interlayer diffusion process. In other metal and semiconductor systems, cooperative exchange,<sup>10,11</sup> kink channel or vacancy diffusion,<sup>12–14</sup> and surfactant-assisted growth<sup>15–17</sup> have been proposed to explain similar discrepancies. Moreover, the possible modification of step-edge barrier due to the interaction between heterogeneous adatoms near step edges can be considered.

Here, as a model system of the vdW epitaxial growth, we study  $\text{Bi}_2\text{Se}_3$ , which is a three-dimensional (3D) topological insulator. Graphene is introduced between the substrate and the thin film as an epitaxial spacer.<sup>18</sup> The graphene layer is most suitable for initial growth because the vdW interaction is weak enough to preserve the inert surface. A quintuple unit of  $\text{Bi}_2\text{Se}_3$  forms a covalent monolayer (ML), which is also stacked periodically by weak vdW interaction (Fig. 1). According to our in situ x-ray diffraction,  $\text{Bi}_2\text{Se}_3$  grew in a smooth multilayer pattern that was expected from the weak vdW interaction. In this study, the evolution of the surface morphology will be explored by a kinetic Monte Carlo (KMC) simulation, using inputs from density functional theory (DFT) calculations.<sup>19–22</sup> Interlayer diffusion processes at step edges are

investigated based on the simplified kinetic multilayer growth model with an additional step-edge barrier.

During multilayer growth, one of the significant factors that determines the film morphology is the additional step-edge barrier  $\Delta E_S$  or Ehrlich–Schwoebel (ES) barrier, which is the difference between the hopping energy barrier  $E_D$  at terraces and  $E_S$  at step edges that governs interlayer diffusion (Fig. 1a).<sup>23,24</sup> Depending on barrier height and growth temperature, different film morphologies develop. High  $\Delta E_S$  hinders the downward diffusion of adatoms at step edges and leads to rough 3D growth. However, if  $\Delta E_S$  is small, the adatoms have sufficient thermal energy to overcome the step-edge barrier, so layer-by-layer (LBL) growth occurs and smooth surfaces are obtained.

## RESULTS

We performed DFT calculations to find the most stable adsorption sites of adatoms and the hopping energy barriers (Fig. 1; see Supplementary information for details of calculation).<sup>3</sup> Atomic positions of two top-surface-layers and edge-nearby atoms are fully relaxed. For a Bi atom adsorption on terrace, two stable configurations are identified as a metastable one with an adsorption energy  $E_{\text{ad}} = -1.28$  eV at a bridge site of Se–Se and the most stable one with  $E_{\text{ad}}^{(\text{Bi})} = -1.50$  eV. For a Se atom, only one stable configuration is found with  $E_{\text{ad}}^{(\text{Se})} = -2.07$  eV (see Supplementary information for details). The transition energy barrier of the Bi adatom from the metastable to the most stable configuration is as small as 0.10 eV from the nudged elastic band (NEB) method calculation.<sup>25</sup> Although these are obtained from the 2D slab model, we obtained nearly the same results by using the ribbon model shown in Fig. 1b, that is, Fig. 1d(i) or (ii) for Bi, Fig. 1e (i) or (ii) for Se.

Migration of the adatoms can be described as a sequence of random hops on a periodic lattice with the binding sites. Transition state theory<sup>26–29</sup> suggests that the activation energies for individual hops are determined by energy differences between

<sup>1</sup>Pohang Accelerator Laboratory, Pohang University of Science and Technology, Pohang, Gyeongbuk 37673, Korea. <sup>2</sup>Department of Chemistry, Ulsan National Institute of Science and Technology, Ulsan 44919, Korea. <sup>3</sup>Department of Ophthalmic Optics, Chodang University, Muan, Jeonnam 58530, Korea. <sup>4</sup>These authors contributed equally: Yongsam Kim, Geunsik Lee. \*email: [kimks@unist.ac.kr](mailto:kimks@unist.ac.kr); [east@postech.ac.kr](mailto:east@postech.ac.kr)

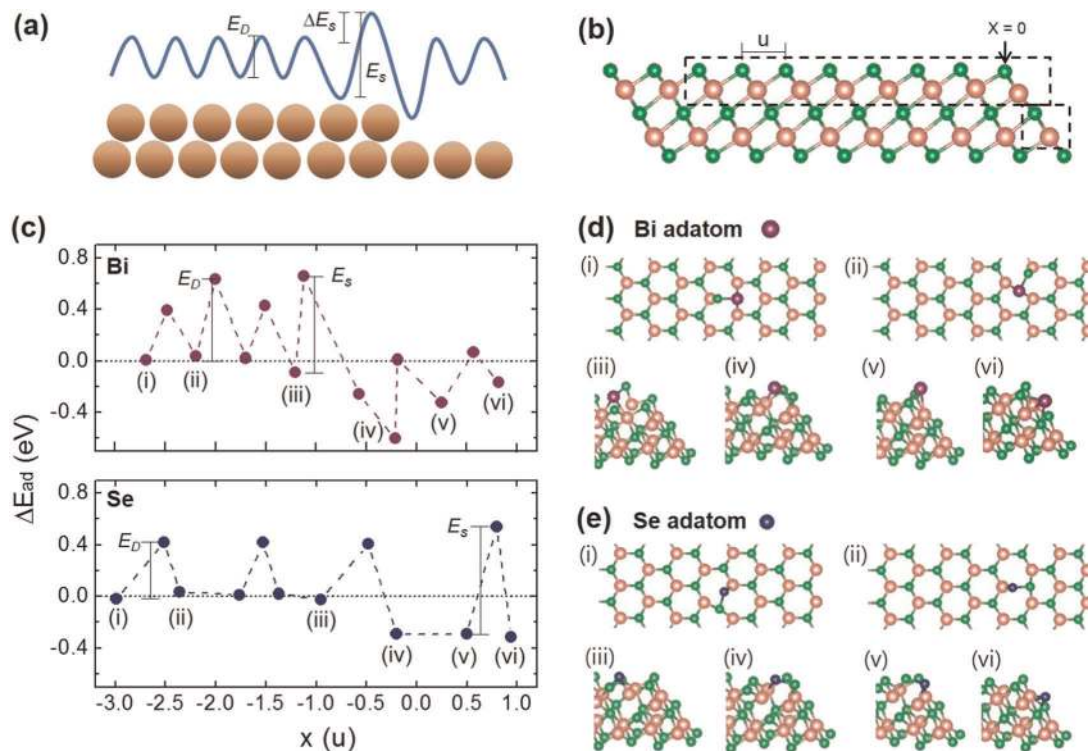


**Fig. 1 Step-edge barrier.** **a** Schematic of energy barriers for usual metallic surface. **b** Atomic model of  $\text{Bi}_2\text{Se}_3$  as a quintuple unit composed of five atomic layers. The dashed rectangles indicate the surface and edge-nearby atoms to be optimized in DFT calculation. **c** Potential energy landscape for the diffusion path displayed by using relative adsorption energies  $\Delta E_{\text{ad}}$ .  $E_D$  is 0.64 eV for Bi and 0.41 eV for Se, and  $\Delta E_S \approx E_S - E_D$  is 0.11 eV for Bi and 0.42 eV for Se ( $u$ : lattice unit). **d, e** The most stable adsorption sites of Bi and Se adatoms. The calculated geometry of the  $\text{Bi}_2\text{Se}_3$  with an adatom. Surface diffusion processes of Bi and Se adatoms on  $\text{Bi}_2\text{Se}_3$  surface toward a step edge ( $X = 0$ ) located at the right side.

the binding and the transition sites. Based on the potential energy landscape obtained from the most stable buckled geometry, the terrace hopping barrier calculated by the 2D slab model is  $E_D = 0.64$  eV for Bi and 0.41 eV for Se adatoms. Actually this barrier corresponds to the energy cost to partially break the Bi–Bi or Se–Se bonds. The step-edge barriers  $E_S$  are calculated using our ribbon model (Fig. 1b; see Supplementary information). Each adatom migrates toward the step edge ( $X = 0$ ) from the inner site ( $X = -3$  lattice units) where the hopping barriers are close to those calculated for the terrace. The relative adsorption energies  $\Delta E_{\text{ad}}$  of Bi and Se diffusing across the edge become higher than  $E_D$ , i.e.,  $E_S = 0.75$  eV for Bi and 0.83 eV for Se (Fig. 1c). Additional step-edge barriers<sup>3,23,24,30</sup>  $\Delta E_S \approx E_S - E_D$ , are as large as 0.11 eV for Bi and 0.42 eV for Se. In this situation, the interlayer diffusion of Se adatoms would be a rate-determining process.

Our DFT calculations yielded the most important hopping barriers on terrace  $E_D$  and step edges  $E_S$ . These two barriers were then used in the construction of the KMC simulation model to simulate growth processes. In the LBL growth regime of a 2D layered material, i.e., the highly diffusive regime of  $D/a^4F \sim 10^8 - 10^{10}$  ( $D$ : diffusion coefficient,  $F$ : deposition rate,  $a$ : lattice constant), we performed KMC simulations with various parameters to reproduce the film growth pattern. The simulation was simplified by assuming that a unit layer on a hexagonal lattice has not a quintuple unit of five atomic layers but monoatomic height with a single species.<sup>19–22</sup> In the KMC code, the surface hopping barrier of an adatom is fixed at  $E_D = 0.4$  eV, and the simulations were performed for various  $\Delta E_S$  to trigger the rate at which atoms cross over step edges into the next lower level. Other periphery diffusions of adatom at island edges were prescribed to produce the triangular islands observed experimentally. At  $T = 500$  K, simulation with  $\Delta E_S = 0.1$  eV yielded LBL growth, whereas simulation with  $\Delta E_S = 0.4$  eV yielded a 3D multilayer pattern

(Fig. 2a). When we used the higher barrier  $\Delta E_S^{\text{(DFT)}} = 0.42$  eV for Se adatoms as the effective step-edge barrier, the film would grow in the form of strong 3D multilayer according to the simulation (Fig. 2b). However, this is unlike the actual case of smooth multilayer growth. This morphological discrepancy was pronounced in the results of x-ray diffraction below.

To examine the layer distribution in detail, in situ x-ray scattering was performed. We grew  $\text{Bi}_2\text{Se}_3$  films epitaxially by thermal evaporation at varying deposition rates  $R_n$  and growth temperatures  $T$  under ultrahigh vacuum.<sup>18</sup> The film growth was performed typically at a relatively slow  $R_n < 0.001$  ML  $\text{s}^{-1}$ . During the film growth, we measured x-ray intensity (Fig. 3a) at an anti-Bragg point at moderate growth temperatures (420–560 K). The observed x-ray intensity was normalized by the initial intensity scattered before the deposition. After the deposition started, the intensity increased up to the high level as much as the first layer is grown. The oscillating anti-Bragg intensity indicates nearly-LBL growth, which is sensitive to morphological changes. Using a simple distributed growth model,<sup>31,32</sup> we fit the data and extracted the coverage  $\theta_n$  of each layer as a function of time.

From the anti-Bragg oscillation, the layer coverages can be retrieved based on a simple rate equation for the coverage change of the  $n$ th layer given by a diffusion equation in the Experimental section (see also Supplementary information). Several analytical fitting models have been developed; they differ in the kinetic parameters used to control the growth, which provide additional information as a result of fitting. We used the Cohen's model, which is a mean-field model that describes morphological evolution during thin film growth.<sup>33</sup> The fitting routine that uses the Cohen's model has been applied successfully to simulate the growth of organic film.<sup>31</sup>

Our experimental anti-Bragg oscillations  $I_{\text{AB}}$  (Fig. 3a) were fitted using  $a_n$  and  $\theta_n(t)$ . The effective distribution of the layer coverage

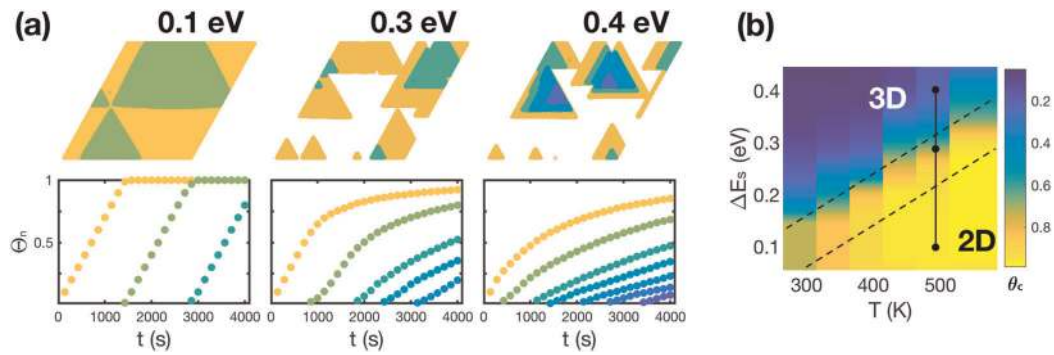


**Fig. 2 KMC simulation.** **a** The KMC simulation of growth for ES barriers  $\Delta E_S = 0.1, 0.3,$  and  $0.4$  eV.  $E_D = 0.4$  eV is used according to the DFT calculation. Experimental temperature  $T = 500$  K and deposition rate  $R_n = 0.0007$  ML  $s^{-1}$  were fixed. The simulated area is a  $600 \times 600$  lattice. **b** Phase diagram of  $\Delta E_S$  vs  $T$ , KMC suggests that 2D and 3D growth separated gradually. Region between dashed lines: smooth multilayer growth.  $\theta_c$ : critical coverage at which a new layer starts to form.

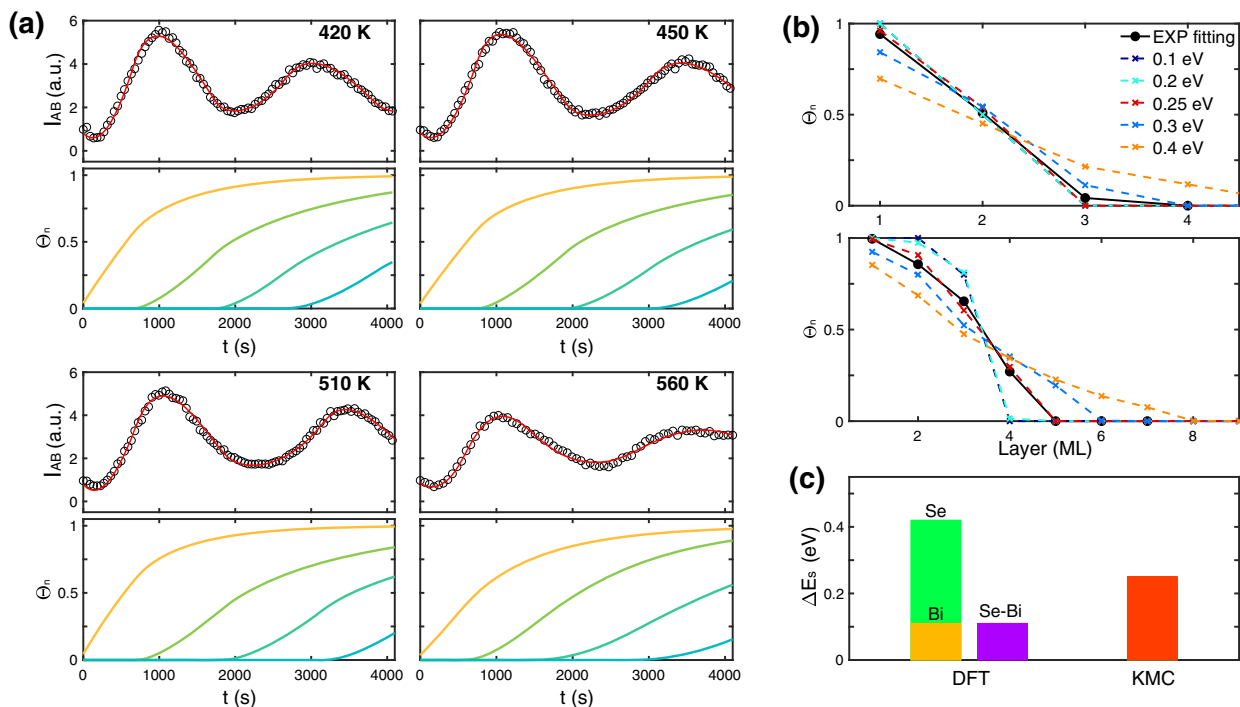


**Fig. 3 Anti-Bragg oscillations.** **a** Anti-Bragg oscillations (open circles) measured at an anti-Bragg  $(00\bar{3})$  position during growth at different temperatures. The layer coverages as a function of the growth time are recovered from the fitting; red curves are best-fits. **b** Experimental layer coverage (black solid line) obtained from anti-Bragg oscillations for total coverage of 1.5 and 2.8 ML, compared with layer profiles (dotted lines) produced by KMC simulations with various ES barriers. **c** The DFT calculations ( $\Delta E_S^{(DFT)}$ ) for ES barriers of single species are much different from the result of the KMC simulation ( $\Delta E_S^{(KMC)}$ ). The DFT barrier for Se–Bi will be discussed in Fig. 4.

$\theta_n(t)$  was deduced from the anti-Bragg fits. Indeed, the  $\theta_n(t)$  in Fig. 3a reveals that  $\text{Bi}_2\text{Se}_3$  film grows rather in smooth multilayers. Furthermore,  $\theta_n$  from the anti-Bragg fit indicates that the effective ES barrier should be  $\Delta E_S^{(KMC)} \sim 0.25$  eV by comparison with the simulated layer coverage profiles (Fig. 3b). Even if the layer coverage profile looks quite similar to the case of  $\Delta E_S^{(KMC)} = 0.25$  eV, the effective  $\Delta E_S^{(KMC)}$  is much different from  $\Delta E_S^{(DFT)} = 0.42$  eV from the DFT calculation.

## DISCUSSION

We now discuss the cause of discrepancy of the above DFT calculation from the effective barrier  $\Delta E_S^{(KMC)}$ . Most effectively, single adatoms were assumed to diffuse on surfaces by simple hopping from one favorable adsorption site to the next on top of

an atomic terrace.<sup>20,21</sup> However, this simple model fails to describe the interlayer diffusion process in our heteroatomic vdW system. Some nontrivial diffusion processes such as exchange processes, surfactants, and downhill diffusions through kink channel or vacancy, might be taken into account as a cause to reduce the energy barriers.<sup>10–17</sup> However, such processes seem to be inapplicable to our system because it possesses quintuple-layered steps that are much different from the usual monoatomic height steps. The relatively wide facet area, at which step edges form, consists of heteroatomic alternating stacked layers. A new diffusion process associated with such a structural feature might be required in order to account for the discrepancy. An adatom that arrives at a laterally growing facet may encounter pre-existing isolated adatoms at step edges. As a secondary process at step edges, a diffusion process that is characterized by the



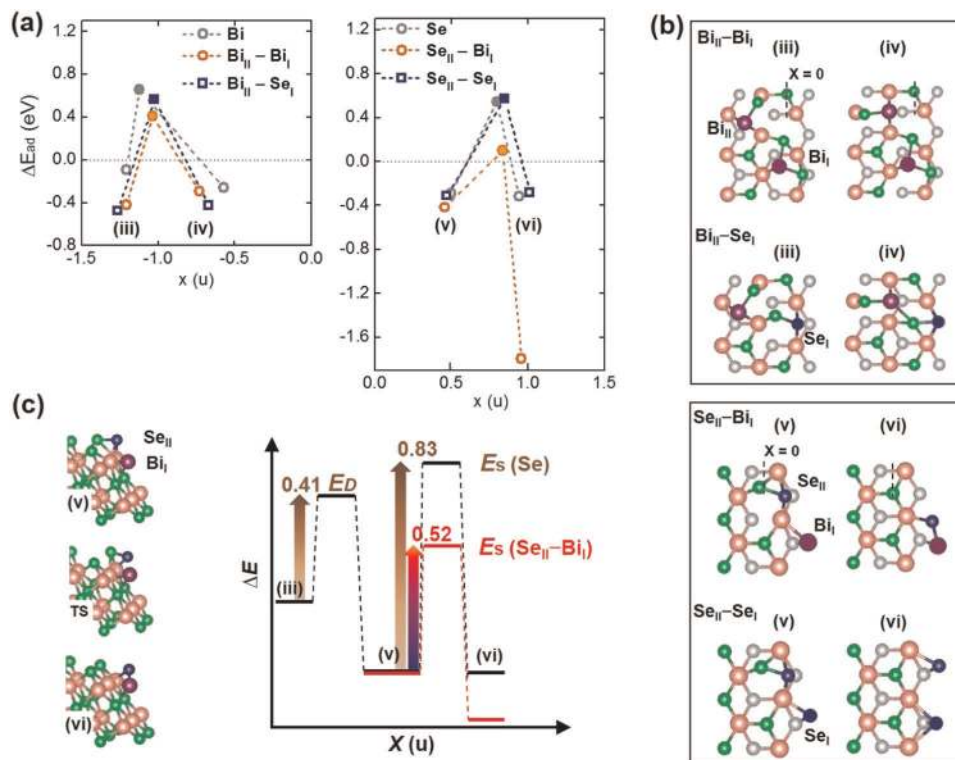


**Fig. 4 Adatom–adatom interaction.** **a** Edge barrier variation for the diffusion of the second  $\text{Bi}_{\text{II}}$  and the second  $\text{Se}_{\text{II}}$  adatom interacting with already-present adsorbed  $\text{Bi}_{\text{I}}$  or  $\text{Se}_{\text{I}}$  adatom nearby (orange circle, blue square); single-adatom edge barrier without adatom–adatom interaction for comparison (gray circle). **b** Initial and final atomic structures for each case, with step edges located at  $X = 0$ . **c** Diffusion process of  $\text{Se}_{\text{II}}$  adatom interacting with  $\text{Bi}_{\text{I}}$  adatom at step sides. TS denotes transition state. The step-edge barrier for  $\text{Se}_{\text{II}}$  adatom is reduced significantly by  $\sim 0.3$  eV compared with single-adatom diffusion so that the reduced ES barrier becomes  $\Delta E_{\text{S}} \sim 0.1$  eV.

heteroatomic interaction between Se and Bi adatoms at step edges might reduce the additional step-edge barrier of  $\Delta E_{\text{S}}^{(\text{Se})} = 0.42$  eV (Fig. 4). In such a process, the Se–Bi adatom interaction would have an important function in crossing over steps. Among various dynamical processes at steps, the most plausible situation would be that a Se adatom approaching a step edge encounters a pre-existing Bi adatom at the step, or vice versa. Indeed, incoming Se adatoms experience a much-reduced ES barrier down to 0.1 eV ( $\Delta E_{\text{S}}^{(\text{Se})} \sim 0.1$  eV) compared to the case of single-adatom diffusion (Fig. 4). A Se adatom diffuses down over the step-edge barrier as easily as if no additional barriers exist. The reduced step-edge barrier affects overall growth pattern significantly. No proper growth model for such heteroatomic systems has been developed so far. However, our DFT result in Fig. 4 emphasizes that the interaction between two heteroatomic species could lower the step-edge barrier. Thus, the heteroatom-assisted reduction of step-edge barrier is strongly reliable for a possible mechanism.

In summary, we performed in situ x-ray scattering to study the growth kinetics of layered  $\text{Bi}_2\text{Se}_3$  film. The x-ray intensity at an anti-Bragg position was fitted using the Cohen's model to obtain kinetic parameters, which reveals an effective step-edge barrier through KMC simulations. Among the step-edge barriers of each diffusing species, large ES barriers should be effectively reduced down to the level of  $\Delta E_{\text{S}}^{(\text{KMC})} \sim 0.25$  eV. The heteroatom-assisted reduction of step-edge barrier drastically modifies the overall growth mechanism for 2D heteroatomic materials. Adatom–adatom interaction may sufficiently reduce high barriers at step edges and such a reduction leads easily to the LBL mode resulting in 2D scalable growth. We thus believe that the new mechanism makes an important step to extend understanding of the kinetics in chemical vapor deposition (CVD) or molecular beam epitaxy (MBE) growth of heteroatomic vdW epitaxial layers.

## METHODS

### DFT calculation

DFT calculations were performed by using the Vienna ab initio simulation package<sup>34</sup> with the PBE-type generalized gradient approximation.<sup>35</sup> A cutoff energy of 210 eV was used for the plane wave expansion. The terrace and edge hopping barriers were calculated by using one quintuple unit of  $\text{Bi}_2\text{Se}_3$  ribbon with the periodic boundary condition along the  $\{100\}$  axis (Fig. 1b; see Supplementary information for details), with sufficient vacuum sizes between periodic images, i.e., 15 Å along  $[210]$  and 13 Å along  $[001]$ . This substrate model is suitable given that commonly observed islands are triangular and that our result with a step edge is most energetically favorable with the fewest dangling bonds. With the four times larger supercell along the  $y$ -direction, the  $k$ -mesh size is  $1 \times 2 \times 1$ . Atomic positions of the two top-surface layers and the edge-nearby atoms in a lattice unit were optimized until the force was  $< 0.02$  eV Å<sup>-1</sup>. The vdW interaction was included by using the Grimme's method, and we also confirmed that the hopping barriers change within the difference of 0.05 eV by using the Tkatchenko–Scheffler dispersion correction. The adsorption energy is defined as

$$E_{\text{ad}} = E_{\text{adsorbed}} - E_{\text{clean}} - E_{\text{atom}}, \quad (1)$$

where  $E_{\text{adsorbed}}$  and  $E_{\text{clean}}$  are the total energies of adsorbed and clean surfaces, respectively, and  $E_{\text{atom}}$  is the total energy of an isolated atom to be adsorbed. Relative adsorption energies,  $\Delta E_{\text{ad}}$ , are defined as the relative values from the terrace adsorption energy. The relative adsorption energies display the potential energy landscape for the diffusion path with the transition state energies found by using the NEB method with the climbing image.<sup>25</sup> Overall accuracy of  $E_{\text{ad}}$  and the hopping barrier is about 0.01 eV. For  $E_{\text{D}}$  and  $E_{\text{S}}$ , we have chosen the largest barrier at terrace—far away from step edge by a few lattice units—and at step edge, respectively.

### KMC simulation

The simulation surface consisted of a lattice of  $600 \times 600$  atoms, in a face-centered cubic (111) surface with straight monoatomic steps.<sup>19</sup> The simulation was simplified by assuming that a unit layer on a hexagonal lattice is a monoatomic layer, rather than a set of five atomic layers. In the

KMC code, the terrace diffusion parameters, such as  $E_D = 0.4$  eV for hopping of a single adatom, an attempt frequency  $\nu_0 = 3 \times 10^{12} \text{s}^{-1}$ , and a deposition rate  $R_n = 0.0007 \text{ ML s}^{-1}$ , were used. To reproduce the experimental triangular islands, other hopping barriers along step edges of island were determined (see Supplementary information for details). We have used effective step-edge barriers because step edges are simplified. Thus, a rate catalog contains a predetermined set of possible configurations and transitions. In addition to diffusion rates and a deposition rate, a sticking coefficient affects the morphological evolution as well. However, the use of such effective barriers simplified on the fcc(111) surface does not affect the morphology of the resulting film significantly.

### X-ray diffraction and anti-Bragg oscillation fitting

Two graphene substrates were prepared: (i) CVD graphene on  $\text{SiO}_2$  and (ii) epitaxial graphene grown on 6H-SiC(0001) surface.<sup>18</sup> The CVD graphene grown on a copper foil was transferred to the  $\text{SiO}_2$  substrate after an etching process. Epitaxial graphene was grown in an ultrahigh vacuum (UHV) chamber. The substrates were mounted in an in situ x-ray scattering chamber at  $< 1 \times 10^{-9}$  Torr.  $\text{Bi}_2\text{Se}_3$  pieces wrapped with tungsten wire were thermally evaporated by heating the tungsten filament resistively. Film growth was performed typically at an effective growth rate ( $< 0.05 \text{ ML min}^{-1}$ ) with the substrate maintained at 420–560 K. During the film growth, intensity oscillations were measured at an anti-Bragg point (0 0 1.5). Measurements were performed at the 5D BL of Pohang Light Source. We performed more than two runs of measurement on each substrate. We collected three effective datasets in total for different substrates, which are within the fit error. The kinetic parameters were obtained using the Cohen's model.<sup>31,32</sup> In this model, adatoms arrive at the film at an effective deposition rate  $R_n$  and adsorb to the surface. Adatoms that land on top of a surface layer may diffuse and incorporate on the uphill steps, or transfer down to the top of the next layer. The rate of change for the coverage  $\theta_n$  of the  $n$ th layer is then given by

$$\frac{d\theta_n}{dt} = R_n(1 - a_{n-1})(\theta_{n-1} - \theta_n) + R_{n+1}a_n(\theta_n - \theta_{n+1}), \quad (2)$$

where  $R_n$  is the effective deposition rate on the  $n$ th layer.  $R_1$  is affected by the sticking probability of substrate.  $a_n$  is the probability of interlayer mass transport into the  $n$ th layer, and measures the rate at which adatoms transfer from the  $(n+1)$ th to the  $n$ th layer.

### DATA AVAILABILITY

The data that support the findings of this study are available from the corresponding author upon reasonable request.

### CODE AVAILABILITY

Detailed information of the used DFT, KMC, and fitting codes is available from the corresponding author upon reasonable request.

Received: 31 August 2019; Accepted: 25 November 2019;  
Published online: 20 December 2019

### REFERENCES

- Venables, J. A., Spiller, G. D. T. & Hanbucken, M. Nucleation and growth of thin films. *Rep. Prog. Phys.* **47**, 399 (1984).
- Brune, H. Microscopic view of epitaxial metal growth: nucleation and aggregation. *Surf. Sci. Rep.* **31**, 121 (1998).
- Michely, T. & Krug, J. *Islands, Mounds, and Atoms: Patterns and Processes In Crystal Growth Far From Equilibrium*. (Springer, Berlin, 2004).
- Evans, J. W., Thiel, P. A. & Bartelt, M. C. Morphological evolution during epitaxial thin film growth: formation of 2D islands and 3D mounds. *Surf. Sci. Rep.* **61**, 1–128 (2006).
- Butler, S. Z. et al. Progress, challenges, and opportunities in two-dimensional materials beyond graphene. *ACS Nano* **7**, 2898–2926 (2013).
- Guo, Y., Liu, Z. & Peng, H. A roadmap for controlled production of topological insulator nanostructures and thin films. *Small* **11**, 3290–3305 (2015).
- Hlawacek, G. et al. Characterization of step-edge barriers in organic thin-film growth. *Science* **321**, 108–111 (2008).
- Bommel, S. et al. Unravelling the multilayer growth of the fullerene  $\text{C}_{60}$  in real time. *Nat. Commun.* **5**, 5388 (2014).

- Ganapathy, R., Buckley, M. R., Gerbode, S. J. & Cohen, I. Direct measurements of island growth and step-edge barriers in colloidal epitaxy. *Science* **327**, 445–448 (2010).
- Kellogg, G. L. & Feibelman, P. J. Surface self-diffusion on Pt(001) by an atomic exchange mechanism. *Phys. Rev. Lett.* **64**, 3143–3146 (1990).
- Feibelman, P. J. Interlayer self-diffusion on stepped Pt(111). *Phys. Rev. Lett.* **81**, 168–171 (1998).
- Lundgren, E., Stanka, B., Leonardelli, G., Schmid, M. & Varga, P. Interlayer diffusion of adatoms: a scanning-tunneling microscopy study. *Phys. Rev. Lett.* **82**, 5068–5071 (1999).
- van Gastel, R., Somfai, E., van Albada, S. B., van Saarloos, W. & Frenken, J. W. M. Nothing moves a surface: vacancy mediated surface diffusion. *Phys. Rev. Lett.* **86**, 1562–1565 (2001).
- Grant, M. L., Swartzentruber, B. S., Bartelt, N. C. & Hannon, J. B. Diffusion kinetics in the Pd/Cu(001) surface alloy. *Phys. Rev. Lett.* **86**, 4588–4591 (2001).
- Esch, S., Hohage, M., Michely, T. & Comsa, G. Origin of oxygen induced layer-by-layer growth in homoepitaxy on Pt(111). *Phys. Rev. Lett.* **72**, 518–521 (1994).
- Camarero, J. et al. Atomistic mechanism of surfactant-assisted epitaxial growth. *Phys. Rev. Lett.* **81**, 850–853 (1998).
- Copel, M., Reuter, M. C., Kaxiras, E. & Tromp, R. M. Surfactants in epitaxial growth. *Phys. Rev. Lett.* **63**, 632–635 (1989).
- Kim, N. et al. Persistent topological surface state at the interface of  $\text{Bi}_2\text{Se}_3$  film grown on patterned graphene. *ACS Nano* **8**, 1154–1160 (2014).
- Seo, J. & Kim, J.-S. Origin of the spontaneous orientational ordering of islands during thin film growth. *Phys. Rev. B* **96**, 085402 (2017).
- Nie, Y. et al. A kinetic Monte Carlo simulation method of van der Waals epitaxy for atomistic nucleation-growth processes of transition metal dichalcogenides. *Sci. Rep.* **7**, 2977 (2017).
- Nie, Y. et al. First principles kinetic Monte Carlo study on the growth patterns of  $\text{WSe}_2$  monolayer. *2D Mater.* **3**, 025029 (2016).
- Rajan, A. G., Warner, J. H., Blankschtein, D. & Strano, M. S. Generalized mechanistic model for the chemical vapor deposition of 2D transition metal dichalcogenide monolayers. *ACS Nano* **10**, 4330–4344 (2016).
- Ehrlich, G. & Hudda, F. G. Atomic view of surface self-diffusion: tungsten on tungsten. *J. Chem. Phys.* **44**, 1039–1049 (1966).
- Schwoebel, R. L. & Shipsey, E. J. Step motion on crystal surfaces. *J. Appl. Phys.* **37**, 3682–3686 (1966).
- Henkelman, G. A climbing image nudged elastic band method for finding saddle points and minimum energy paths. *J. Chem. Phys.* **113**, 9901–9904 (2000).
- Marcelin, R. Contribution à l'étude de la cinétique physico-chimique. *Ann. Phys.* **3**, 120–231 (1915).
- Eyring, H. The activated complex in chemical reactions. *J. Chem. Phys.* **3**, 107–115 (1935).
- Vineyard, G. H. Frequency factors and isotope effects in solid state rate processes. *J. Phys. Chem. Solids* **3**, 121 (1957).
- Voter, A. F. & Doll, J. D. Transition state theory description of surface self-diffusion: Comparison with classical trajectory results. *J. Chem. Phys.* **80**, 5832 (1984).
- Kyuno, K. & Ehrlich, G. Step-edge barriers: truths and kinetic consequences. *Surf. Sci.* **383**, L766–L774 (1997).
- Woll, A. R., Desai, T. V. & Engstrom, J. R. Quantitative modeling of in situ x-ray reflectivity during organic molecule thin film growth. *Phys. Rev. B* **84**, 075479 (2011).
- Cohen, P. I., Petrich, G. S., Pukite, P. R., Whaley, G. J. & Arrott, A. S. Birth-death models of epitaxy. *Surf. Sci.* **216**, 222–248 (1989).
- Tomellini, M. & Fanfoni, M. Mean field approach for describing thin film morphology. *J. Phys. Condens. Matter* **18**, 4219 (2006).
- Kresse, G. & Furthmüller, J. Efficiency of ab-initio total energy calculations for metals and semiconductors using a plane-wave basis set. *Comput. Mater. Sci.* **6**, 15–50 (1996).
- Perdew, J. P., Burke, K. & Ernzerhof, M. Generalized gradient approximation made simple. *Phys. Rev. Lett.* **77**, 3865 (1996).

### ACKNOWLEDGEMENTS

This work was supported by the National Research Foundation of Korea (NRF) grant funded by the Korean government (NRF-2016R1C1B1007232, 2018R1D1A1B07045180, National Honor Scientist Program: 2010-0020414, 2018R1D1A1B07045983, 2018R1D1A1B07045310). Computation was supported by KISTI (KSC-2018-CRE-0077, KSC-2019-CRE-0103).

### AUTHOR CONTRIBUTIONS

Y.K. and N.K. designed and conducted the experiment. G.L. and N.L. performed the DFT calculation. Y.K., N.K., and J.S. performed the KMC simulation. Y.K., G.L., K.S.K., and N.K. wrote the manuscript. Y.K. and G.L. contributed equally to this work.

### COMPETING INTERESTS

The authors declare no competing interests.

### ADDITIONAL INFORMATION

**Supplementary information** is available for this paper at <https://doi.org/10.1038/s41699-019-0134-2>.

**Correspondence** and requests for materials should be addressed to K.S.K. or N.K.

**Reprints and permission information** is available at <http://www.nature.com/reprints>

**Publisher's note** Springer Nature remains neutral with regard to jurisdictional claims in published maps and institutional affiliations.



**Open Access** This article is licensed under a Creative Commons Attribution 4.0 International License, which permits use, sharing, adaptation, distribution and reproduction in any medium or format, as long as you give appropriate credit to the original author(s) and the source, provide a link to the Creative Commons license, and indicate if changes were made. The images or other third party material in this article are included in the article's Creative Commons license, unless indicated otherwise in a credit line to the material. If material is not included in the article's Creative Commons license and your intended use is not permitted by statutory regulation or exceeds the permitted use, you will need to obtain permission directly from the copyright holder. To view a copy of this license, visit <http://creativecommons.org/licenses/by/4.0/>.

© The Author(s) 2019